Progress In Electromagnetics Research, PIER 104, 69–83, 2010

TRANSFER FUNCTION AND COMPACT DISTRIBUTED RLC MODELS OF CARBON NANOTUBE BUNDLE INTERCONNETS AND THEIR APPLICATIONS

J. P. Cui and W.-Y. Yin

Center for Optical and Electromagnetic Research (COER)
State Key Lab of MOI
Zhejiang University
Hangzhou 310058, China

Abstract—According to the derived transfer function using different orders of approximation, stability and signal transmission analysis of a driven metallic single-walled carbon nanotube (SWCNT) bundle interconnect are performed. It is shown that as the length of SWCNT bundle interconnect increases, the poles will be closer to the imaginary axis, which causes the transmitted signal response tends to be more damping. Using the fourth-order approximation of the transfer function, the transmitted pulse waveform along the SWCNT bundle interconnect is captured accurately, with signal overshoot and time delay examined. Further, a complete physical model for the transient response of carbon nanotube bundle interconnect is derived, which can also accurately predict the transient response of carbon nanotube bundle interconnect including time delay and crosstalk.

1. INTRODUCTION

Due to their unique features of high current carrying capability, excellent thermal and mechanical properties, carbon nanotubes (CNT) have drawn much attention in the development of future interconnects in the past several years [1]. Significant research progresses have been achieved in modeling single-, double-, and multi-walled CNT (SWCNT, DWCNT and MWCNT) interconnects. These progresses mainly include: (a) the development of RF circuit models for single and bundle interconnects consisting of SWCNT, DWCNT and MWCNT [2–5]; (b) the extraction of their distributed parameters [6–8]; (c) the characterization of crosstalk effects [9, 10], (d) the prediction of their

Corresponding author: W.-Y. Yin (wyyin@zju.edu.cn).

performance parameters in comparison with copper interconnects used for advanced CMOS fabrication technologies [11–13], and (e) the study on their relative stability [14], power handling capability, and other reliability issues [15]. On the other hand, it must be emphasized that design and fabrication technologies of CNT-based interconnects are very important for their real application in the future 3-D ICs, and some significant progresses can be found in [15–19]. Also, some methodologies on transmission line, interconnects and transient signal analysis can be found in [30–32].

It is also known that as the transfer function of an on-chip interconnect in the Laplace domain is obtained, its inductance effects, transferred signal stability, and output response excited by an arbitrary signal can be determined accurately [20]. The fourth-order approximation is often used in the derivation of transfer function. To the best of our knowledge, although relative stability analysis of CNT bundle is presented in [14] with Nyquist stability criterion implemented, no one addresses the solution to its absolute stability problem which is also important for the design of CNT-based networks.

Further, we know that compact distributed RLC models are always essential for the design and global optimization of multilevel interconnect networks. Fortunately, a set of distributed RLC models for copper interconnects, after tedious mathematical treatment, has been developed by Davis and Venkatesan [21–24]. With it, we can accurately and quickly capture time delay, overshoot, crosstalk, and repeater insertion of single and coupled copper interconnects, respectively.

In this paper, absolute stability analysis of SWCNT bundle interconnects will be carried out at first, based on the derived transfer function in the Laplace domain and its pole distribution. Then, using the method of special functions proposed in [21–24], some compact distributed RLC models for SWCNT bundle interconnects are derived, and their successful applications in predicting bundle transmission characteristics are demonstrated, such as crosstalk effect.

2. TRANSFER FUNCTION AND ABSOLUTE STABILITY

Figure 1(a) shows a SWCNT bundle interconnect of length l_{th} on a double-layered substrate of silicon oxide and silicon. Its equivalent distributed circuit model is shown in Fig. 1(b). Because of the present limitation in fabrication technology, a SWCNT bundle is often a mixture of metallic CNTs and semiconducting ones [10]. Here, we use P_m donates the metallic probability of a SWCNT in the bundle

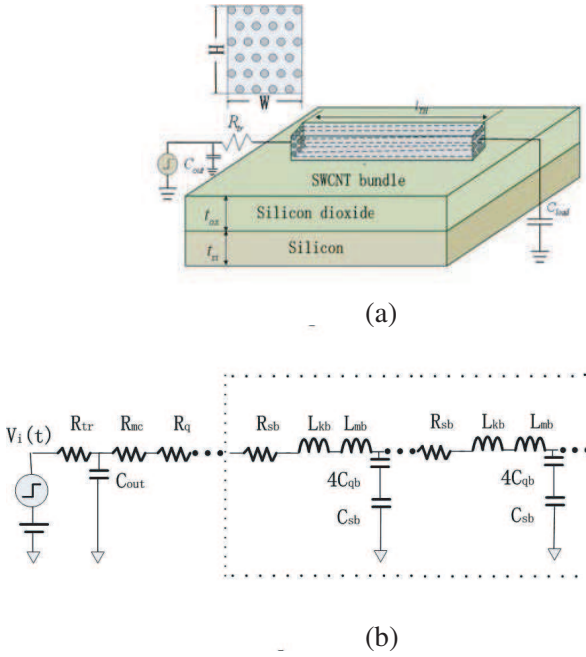

Figure 1. (a) Geometry of a SWCNT bundle interconnect; and (b) its equivalent distributed circuit model.

$(0 < P_m \leq 1)$, with the metallic tube number denoted by n_{CNT}, and

$$n_{CNT} = P_m(n_H n_W - \lfloor n_H/2 \rfloor) \tag{1a}$$

$$n_W = \text{Inter}\left[(W - D)/(D + \Delta)\right] + 1 \tag{1b}$$

$$n_H = \text{Inter}\left[(H - D)/((\sqrt{3}/2)(D + \Delta))\right] + 1 \tag{1c}$$

where n_H and n_W are the tube numbers in the vertical and horizontal directions [4], respectively; "Inter [ ]" indicates that only the integer part is taken into account; D and $\Delta(= 0.34\,\text{nm}\ [1, 4])$ denote the diameter of each metallic tube and the separation between two neighbouring tubes in the bundle, respectively.

In Fig. 1(b), R_{tr} and C_{out} are the equivalent resistance and output capacitance of the driver at the input port, C_{load} is the loaded capacitance at the output port, and R_{mc} denotes the metal-CNT contact resistance introduced by fabrication. The intrinsic resistance R_{sb} and the quantum one R_q are calculated by [10]

$$R_{sb} = R_q/(\lambda_{CNT} n_{CNT}) = h/\left(4e^2 \lambda_{CNT} n_{CNT}\right) \tag{2a}$$

$$R_q = h/(4e^2) \tag{2b}$$

where the value of R_q is 6.4 kΩ, with electron spin degeneracy considered, and λ_{CNT} is the mean free path (mfp). For a SWCNT bundle, there are per-unit-length kinetic and magnetic inductances, denoted by L_{kb} and L_{mb}, respectively. The per-unit-length electrostatic and quantum capacitances of the bundle are represented by C_{sb} and C_{qb}, respectively. The magnetic inductance L_{mb} and electrostatic capacitance C_{sb} of the bundle can be obtained just by calculating the inductance and capacitance of a copper wire but with the same cross-sectional dimensions instead. The kinetic inductance L_{kb} and quantum capacitance C_{qb} of the bundle are calculated by

$$L_{kb} = L_{k-CNT}/n_{CNT} = h/\left(2e^2 v_F\right) n_{CNT} \tag{3}$$

$$C_{qb} = C_q n_{CNT} = 2e^2 n_{CNT}/(h v_F) \tag{4}$$

where v_F is the Fermi velocity. We would like to say that, since the total inductance is dominated by the kinetic term, the magnetic coupling among tubes can be excluded.

In Fig. 1(a), as $l_{th} \gg \lambda_{CNT}$, the input-output transfer function of the bundle in the Laplace domain can be calculated by [25]

$$H(s) = \left\{[1 + sR_{tr}(C_{out} + C_L)]\cosh(\theta l_{th}) + \left(R_{tr}/Z_0^T + sZ_0^T C_L + s^2 Z_0^T R_{tr} C_{out} C_L\right)\sinh(\theta l_{th})\right\}^{-1} \tag{5}$$

where $Z_0^T = \sqrt{(R_{sb} + sL_b)/sC_b}$, $\theta = \sqrt{(R_{sb} + sL_b)sC_b}$, and $s = j\omega$ is the complex frequency. As we expand $\cosh(\theta l_{th})$ and $\sinh(\theta l_{th})$ into infinite series and collect the terms up to the coefficient of s^6 in the denominator, we can express the transfer function as [25, 26]

$$H(s) = 1/\left[1 + \sum_{m=1}^{M} b_m s^m\right] \tag{6a}$$

where $b_m (m = 1, \ldots,$ and 6) are given by:

$$b_1 = R_{tr}(C_{out} + C_L) + R_{sb}C_b l_{th}^2/(2!) + R_{tr}C_b l_{th} + C_L R_{sb} l_{th} \tag{6b}$$

$$\begin{aligned} b_2 = {} & L_b C_b l_{th}^2/(2!) + R_{sb}^2 C_b^2 l_{th}^4/(4!) + C_b R_{tr}(C_{out} + C_L) R_{sb} l_{th}^2/(2!) \\ & + R_{sb} C_b l_{th}^2 (R_{tr} C_b l_{th} + C_L R_{sb} l_{th})/(3!) \\ & + C_L L_b l_{th} + R_{tr} C_{out} C_L R_{sb} l_{th} \end{aligned} \tag{6c}$$

$$\begin{aligned} b_3 = {} & 2R_{sb} L_b C_b^2 l_{th}^4/(4!) + R_{sb}^3 C_b^3 l_{th}^6/(6!) + R_{tr} l_{th}^2 C_b \cdot (C_{out} + C_L)(L_b/(2!) \\ & + R_{sb}^2 C_b l_{th}^2/(4!)) + l_{th}^3 C_b (R_{tr} C_b + C_L R_{sb}) \cdot (L_b/(3!) \\ & + R_{sb}^2 C_b l_{th}^2/(5!)) + (L_b + R_{tr} C_{out} R_{sb}) C_L L_b C_b l_{th}^3/(3!) \\ & + R_{tr} C_{out} C_L L_b l_{th} \end{aligned} \tag{6d}$$

$$
\begin{aligned}
b_4 = {} & L_b^2 C_b^2 l_{th}^4/(4!) + 3L_b R_{sb}^2 C_b^3 l_{th}^6/(6!) + R_{sb}^4 C_b^4 l_{th}^8/(8!) \\
& + R_{tr} R_{sb} C_b^2 l_{th}^4 (C_{out} + C_L)(2L_b/(4!) + C_b R_{sb}^2 l_{th}^2/(6!)) \\
& + R_{sb} C_b^2 l_{th}^4 (R_{tr} C_b l_{th} + C_L R_{s-b} l_{th})(C_b l_{th}^2 R_{sb}^2/(7!) + 2L_b/(5!)) \\
& + C_b C_L l_{th}^3 (L_b + C_{out} R_{sb} R_{tr})(L_b/(3!) + C_b R_{sb}^2 l_{th}^2/(5!)) \\
& + C_b C_L C_{out} L_b R_{sb} R_{tr} l_{th}^3/(3!) \qquad (6e) \\
b_5 = {} & 3L_b^2 C_b^3 R_{sb} l_{th}^6/(6!) + 4L_b R_{sb}^3 C_b^4 l_{TH}^8/(8!) + R_{sb}^5 C_b^5 l_{th}^{10}/(10!) \\
& + R_{tr} C_b^2 l_{th}^4 (C_{out} + C_L)(L_b^2/(4!) + 3R_{sb}^2 L_b C_b l_{th}^2/(6!) \\
& + R_{sb}^4 C_b^2 l_{th}^4/(8!)) + R_{tr} C_b^3 l_{th}^5 (L_b^2/(5!) + 3C_b L_b R_{sb}^2 l_{th}^2/(7!) \\
& + C_b^2 R_{sb}^4 l_{th}^4/(9!)) + R_{sb} C_L C_b^2 l_{th}^5 (L_b^2/(5!) + 3C_b L_b R_{sb}^2 l_{th}^2/(7!) \\
& + C_b^2 R_{sb}^4 l_{th}^4/(9!) + C_L L_b R_{sb} C_b^2 l_{th}^5 (2L_b/(5!) + R_{sb}^2 C_b l_{th}^2/(7!)) \\
& + R_{tr} C_L C_{out} C_b^2 R_{sb}^2 l_{th}^5 (2L_b/(5!) + C_b l_{th}^2/(7!)) \\
& + C_b C_L C_{out} L_b R_{tr} l_{th}^3 (L_b/(3!) + C_b R_{sb}^2 l_{th}^2/(5!)) \qquad (6f) \\
b_6 = {} & C_b^3 L_b^3 l_{th}^6/6! + 6L_b^2 R_{sb}^2 C_b^4 l_{th}^8/8! + 5C_b^5 L_b R_{sb}^4 l_{th}^{10}/10! + R_{sb}^6 C_b^6 l_{th}^{12}/(12!) \\
& + R_{sb} R_{tr} C_b^3 l_{th}^6 (C_{out} + C_L)(3L_b^2/6! + C_b^2 R_{sb}^4 l_{th}^4/10! \\
& + 4C_b R_{sb}^2 L_b l_{th}^2/8!) + R_{sb} R_{tr} C_b^4 l_{th}^7 3L_b^2/7! + C_b^2 R_{sb}^4 l_{th}^4/11! \\
& + 4C_b L_b R_{sb}^2 l_{th}^3/9! + C_L L_b R_{sb}^2 C_b^3 l_{th}^7 (3L_b/7! + 4R_{sb}^2 C_b l_{th}^2/9!)) \\
& + C_L L_b C_b^2 l_{th}^5 (L_b^2/(5!) + 3C_b L_b R_{sb}^2 l_{th}^2/(7!) + C_b^2 R_{sb}^4 l_{th}^4/(9!)) \\
& + C_L C_{out} R_{sb} R_{tr} C_b^2 l_{th}^5 (L_b^2/(5!) + 3C_b L_b R_{sb}^2 l_{th}^2/7! + C_b^2 R_{sb}^4 l_{th}^4/(9!)) \\
& + C_L C_{out} L_b R_{sb} R_{tr} C_b^2 l_{th}^5 (2L_b/(5!) + C_b R_{sb}^2 l_{th}^2/(7!) \qquad (6g)
\end{aligned}
$$

Using (6a)–(6g), both relative and absolute stability of the SWCNT bundle interconnects can be predicted numerically.

3. COMPACT DISTRIBUTED RLC MODEL OF CNT BUNDLE INTERCONNECTS

Figures 2(a) and 2(b) show the cross-sectional views of two on-chip CNT bundle interconnects, and they can be made of SWCNTs, DWCNTs, and even MWCNTs.

According to the method of special function proposed in [23], we now extend the compact distributed RLC model for normal metallic interconnects to CNT bundle cases. In Fig. 2(a), the voltage at the signal (S) bundle end, denoted by $V_{fin}(l_{th}, s)$ in the Laplace domain, can also be described by [23]:

$$V_{fin}(x = l_{th}, s) = (1 + \Gamma_L) \sum_{n=0}^{g} \left[\Gamma_L^n \Gamma_S^n V_{\inf}((2n+1) l_{th}, s) \right] \qquad (7)$$

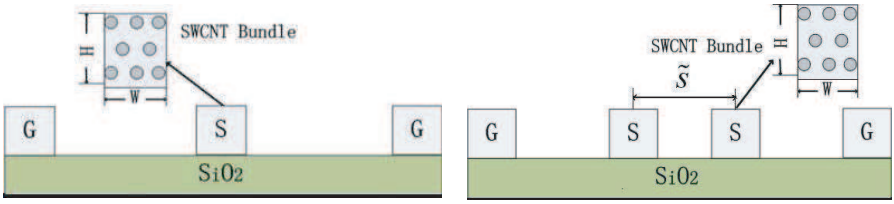

Figure 2. Cross-sectional views of two on-chip CNT bundle interconnects: (a) Ground(G)-signal(S)-Ground(G); and (b) G-S-S-G.

and

$$g = \left\langle 0.5\left(\left(t/l_{th}\sqrt{L_bC_b}\right)+1\right)\right\rangle - 1.0 \tag{8a}$$

$$\mathrm{V}_{\inf}(x,s) = \frac{V_{dd}}{s}\frac{Z_o\sqrt{(s+R_b/L_b)/s}}{Z_o\sqrt{(s+R_b/L_b)/s}+R_{tr}}e^{-x\sqrt{L_bC_b}\sqrt{s(s+R_b/L_b)}} \tag{8b}$$

where R_b, L_b and C_b are the per-unit-length resistance, inductance and capacitance, respectively; g is the reflection number of the transmitted signal along the CNT bundle, $\mathrm{V}_{\inf}(l_{th},s)$ is the voltage in the Laplace domain at the coordinate x of the bundle, but with an infinite length assumed; and V_{dd}/s is the Laplace equivalent of the step input signal, Γ_S and Γ_L are the reflection coefficients at the source and capacitance load ends, respectively, which are defined as

$$\Gamma_S = \frac{Z_S - Z(s)}{Z_S + Z(s)} = \frac{R_{tr} - Z_o\sqrt{1+R_b/(sL_b)}}{R_{tr} + Z_o\sqrt{1+R_b/(sL_b)}} \tag{9}$$

$$\Gamma_L = \frac{Z_L - Z(s)}{Z_L + Z(s)} = \frac{1 - sC_LZ_o\sqrt{1+R_b/(sL_b)}}{1 + sC_LZ_o\sqrt{1+R_b/(sL_b)}} \tag{10}$$

where $Z_o = \sqrt{L_b/C_b}$ is the characteristic impedance of the CNT bundle, and $Z_L = 1/(sC_{load})$. Following the similar way as used in [23], (7) can be decoupled as

$$V_{fin}(x = l_{th}, s) = V_1(s) + V_2(s) \tag{11}$$

and $V_1(s)$ is the first reflection ($n = 0$) term given by

$$V_1(s) = (1+\Gamma_L)\,\mathrm{V}_{\inf}(l_{th},s) \tag{12}$$

$V_2(s)$ is the second- and higher-order reflection ($n \geq 1$) term given by

$$V_2(s) = \sum_{n=1}^{g}\left[\left(\Gamma_L^n\Gamma_S^n + \Gamma_L^{n+1}\Gamma_S^n\right)\mathrm{V}_{\inf}((2n+1)\,l_{th},s)\right] \tag{13}$$

Using the inverse Laplace transform, the voltage response in the time domain can be obtained by

$$V_{fin}(l_{th},t) = V_1(t) + V_2(t) \tag{14}$$

As discussed in [23], (14) also consists of three separate models as follows:

$$\text{Model 1}: \; V_{fin}(l_{th},t) = e^{-R_b t/(2L_b)}\left(V'_{1A}(t) + V'_{2A}(t)\right) \tag{15}$$

$$\text{Model 2}: \; V_{fin}(l_{th},t) = e^{-R_b t/(2L_b)}\left(V'_{1B}(t) + V'_{2A}(t)\right) \tag{16}$$

$$\text{Model 3}: \; V_{fin}(l_{th},t) = e^{-R_b t/(2L_b)}\left(V'_{1B}(t) + V'_{2B}(t)\right) \tag{17}$$

And the model choice depends on certain convergence rules as proposed in [23].

In Fig. 2(b), the decoupled partial differential equation (PDE) for the common and differential modes of voltage wave propagation in two-coupled CNT bundle interconnects can be described by a set of similar equations as given in [23], and

$$\frac{\partial^2}{\partial x^2}V_+(x,t) = (L_{s-b}+L_{m-b})C_{g-b}\frac{\partial^2}{\partial t^2}V_+(x,t) + R_b C_{g-b}\frac{\partial}{\partial t}V_+(x,t) \tag{18a}$$

$$\frac{\partial^2}{\partial x^2}V_-(x,t) = (L_{s-b}-L_{m-b})(C_{g-b}+2C_{m-b})\frac{\partial^2}{\partial t^2}V_-(x,t) + R_b(C_{g-b}+2C_{m-b})\frac{\partial}{\partial t}V_-(x,t) \tag{18b}$$

and

$$V_+(x,t) = V_{fin}(R_b, L_{s-b}+L_{m-b}, C_{g-b}, x, t) \tag{19a}$$

$$V_-(x,t) = V_{fin}(R_b, L_{s-b}-L_{m-b}, C_{g-b}+2C_{m-b}, x, t) \tag{19b}$$

where L_{s-b} and L_{m-b} represents self and mutual inductances of the CNT bundle, respectively. C_{g-b} and C_{m-b} represents bundle to ground and bundle to bundle capacitances, respectively. The approximate expressions for the mutual inductance of CNT bundle is given by [27]

$$L_{m-b} = \frac{\mu}{2\pi}\ln\sqrt{\left(\tilde{s}^2 + (2(a+t_{ox})-a)^2\right)/\tilde{s}^2 + a^2} \tag{20}$$

where t_{ox} is the thickness of SiO_2, a is the equivalent radius of the bundle, $\tilde{s}$ is the centre-to-centre spacing. The bundle to bundle capacitance is calculated by some special methods, such as those proposed in [15]

$$C_{m-b} = \frac{\pi\varepsilon}{\cosh^{-1}((\tilde{s}+D)/D)} \bullet n_{CNT} \tag{21}$$

The transient solutions for the active and quiescent line are given by [23]

$$V_A(x,t) = [V_+(x,t) + V_-(x,t)]/2 \tag{22}$$

$$V_Q(x,t) = [V_+(x,t) - V_-(x,t)]/2 \tag{23}$$

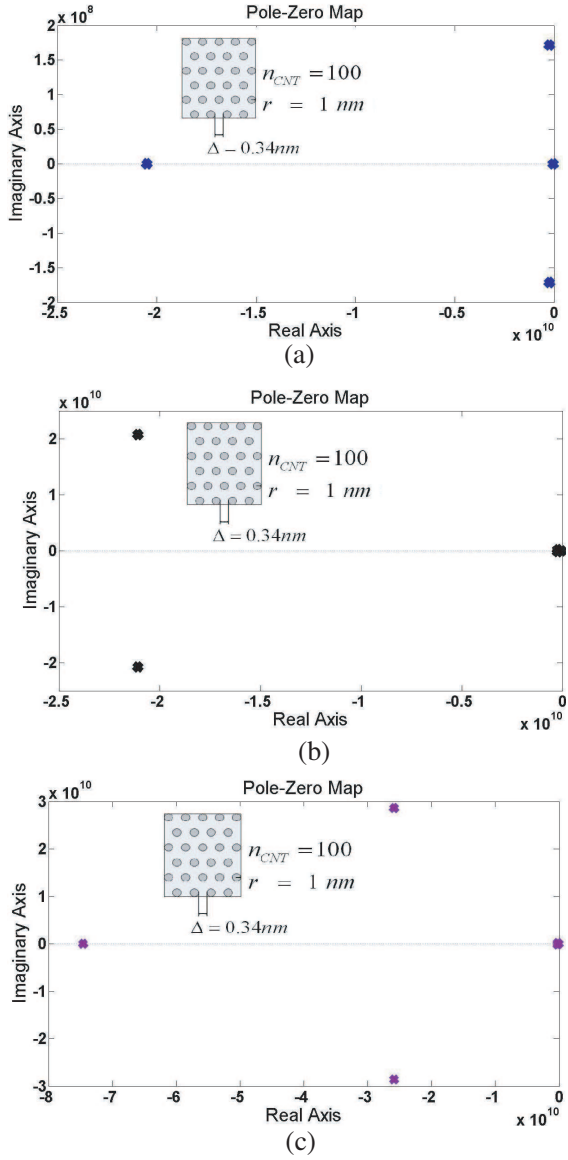

Figure 3. The pole distribution diagrams of a driven SWCNT bundle interconnect using the (a) fourth-, (b) fifth-, and (c) sixth-order approximation of transfer function, respectively.

4. STABILITY ANALYSIS AND RESPONSESOF CNT BUNDLES

4.1. System Stability Analysis

The stability of a SWCNT bundle interconnect can be characterized according to its pole distribution. Figs. 3(a), (b) and (c) show the extracted pole distribution diagrams of a driven SWCNT bundle interconnect using the fourth-, fifth-, and sixth-order approximations of the transfer function, respectively. The diameter of each metallic SWCNT and the number of metallic nanotubes in a given bundle are chosen to be 1nm and 100, respectively. The separation between two neighbouring SWNCTs in the bundle is kept to be 0.34 nm. It is obvious that all poles are located at the left side of the S-plane, so the SWCNT interconnect-based system is always stable.

Figure 4 shows the pole distribution diagram of a driven SWCNT bundle interconnect for different lengths using the fourth-order approximation, with l_{th} = 30, 50, 80, and 1000 m, respectively. It is shown that as the length of SWCNT bundle interconnect increases, the poles will be closer to the imaginary axis, which causes the transmitted signal response tends to be more damping, as also indicated in [14].

4.2. Responses of CNT Bundle

Based on the above input-output transfer function using the third-, fourth-, fifth-, and sixth-order approximations, respectively, we want to predict time-domain responses of a SWCNT bundle interconnect input by a rectangle-like signal. The SWCNT bundle interconnect is driven

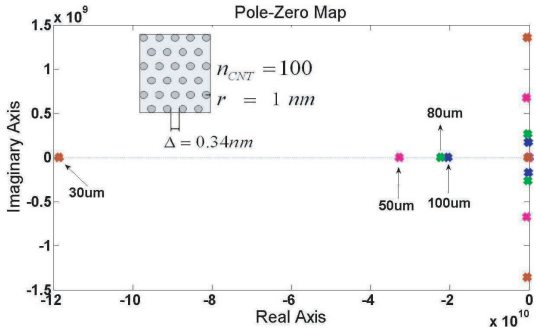

Figure 4. The pole distribution diagram of a driven SWCNT bundle interconnect for different lengths using the fourth-order approximation of transfer function.

by a driver with an equivalent output resistance of the gate driver R_s, and terminated by a load with capacitance C_{load}, as shown in Fig. 1. The other parameters are chosen to be: $R_s = 457\,\Omega$, $C_{load} = 1\,\text{pF}$, $C_{out} = 1\,\text{fF}$, and $n_{CNT} = 100$.

In Fig. 5, it is evident that the output waveforms obtained using the second-, the third-, and the fourth-order approximations of the transfer function are different, with different overshoot and time delay observed. Evidently, the higher the order of the transfer function used, the more accurate the captured pulse waveform is. However, the maximum relative error in the captured pulse waveforms between the third- and fourth-order approximations is only about 0.042%. As we further employ the fifth- and sixth-order approximation of transfer function, the same output waveform is recorded, as compared with that of the fourth-order approximation.

Figure 6 shows the responses of a SWCNT bundle interconnect excited by a rectangular pulse with $l_{th} = 1$, 20, 50, and 100 µm, respectively, and the fourth-order approximation of the transfer function is used in our calculation. It is evident that with increasing the SWCNT bundle length, its resistance effect becomes dominant. As the value of l_{th} increases from 1 to 20, 50 and 1000 m, the time delay of the transmitted pulse is increased from 5.05, 5.18, 7.21, and 23.28 ns gradually.

Further, Fig. 7 shows the time delay of the transmitted pulse as a function of the SWCNT bundle length.

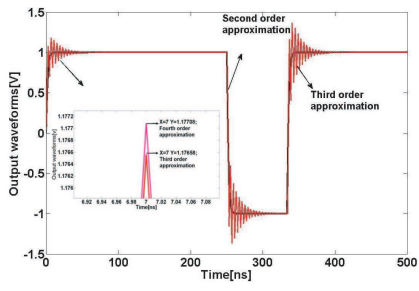

Figure 5. Responses of a SWCNT bundle interconnect excited by a rectangular pulse with a length of 20 µm obtained using the second-, third-, and fourth-order approximations of transfer function, respectively.

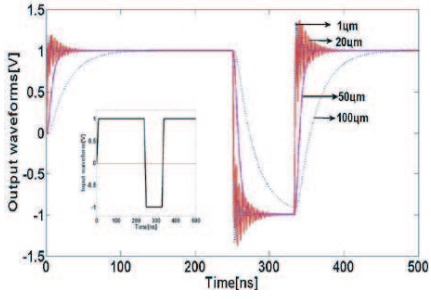

Figure 6. Responses of a SWCNT bundle interconnect excited by a rectangular pulse for different lengths obtained using the fourth-order approximation of transfer function.

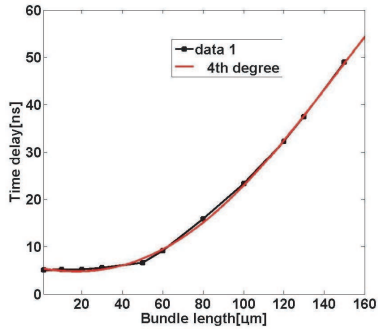

Figure 7. Time delay of the transmitted pulse as a function of SWCNT bundle length using the fourth-order approximation of transfer function, where the fitted red line is obtained using the fourth degree polynomial.

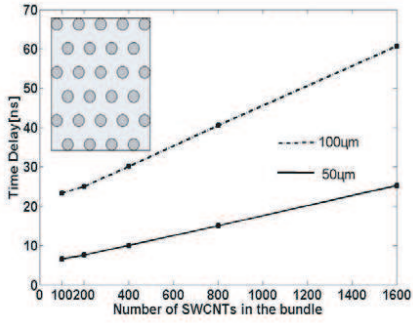

Figure 8. Time delay of the transmitted pulse as a function of the metallic number of SWCNTs in the bundle for different SWCNT bundle lengths using the fourth-order approximation of transfer function.

Based on a lot of numerical experiments, it is found that the time delay of the pulse waveform can be described by the fourth degree polynomial, i.e.,

$$t_d = \sum_{n=0}^{4} a_n l_{th}^n \tag{24}$$

where the polynomial fitting coefficients $a_0 = 5.4$, $a_1 = -0.069$, $a_2 = 0.0017$, $a_3 = 1.4 \times 10^{-5}$, and $a_4 = -5.9 \times 10^{-8}$.

Finally, Fig. 8 shows the time delay as a function of the CNT number in the bundle for its different lengths. It is evident that the time delay (t_d) increases linearly with the value of n_{CNT}.

According to the time domain expression $V_{1A}^{'}(t)$, $V_{2A}^{'}(t)$, $V_{1B}^{'}(t)$ and $V_{2B}^{'}(t)$ which are shown in [29], we can get the output transient response of CNT bundle interconnect for a step input waveform. Fig. 9. shows Output transient responses of a 20 μm CNT bundle interconnect excited by a step input waveform using the complete model for 22-nm technology node.

Figure 10 shows the crosstalk induced in the active and quiescent lines, and the mutual inductance and the bundle to bundle capacitance have certain effect on the crosstalk between two SWCNT bundle interconnects. On the other hand, we would like to say that skin effect in the CNT bundle interconnect is exclude in our study, since the signal

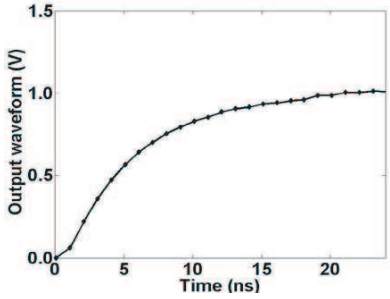

Figure 9. The output voltage of a 200 µm CNT bundle interconnect excited by a step input waveform using the complete model, with $W = 22\,\text{nm}$, $H = 44\,\text{nm}$, $R_b = 1.095e5\,\Omega/\text{cm}$, $C_b = 135.45\,\text{pF/cm}$, $L_b = 70.2\,\text{nH/cm}$, and $C_{load} = 5\,\text{fF}$.

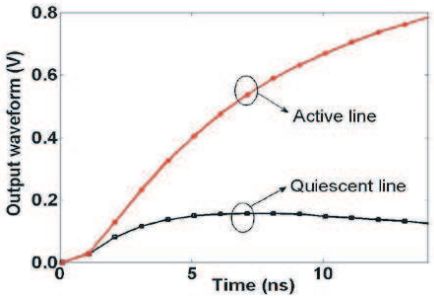

Figure 10. The output voltages of 300-µm-long active and quiescent lines with a step input, and $W = 22\,\text{nm}$, $H = 44\,\text{nm}$, $\tilde{s} = 44\,\text{nm}$, $R_b = 1.095e5\,\Omega/\text{cm}$, $C_{g-b} = 135.45\,\text{pF/cm}$, $L_{s-b} = 70.2\,\text{nH/cm}$, $L_{m-b} = 1.6262\,\text{nH/cm}$, $C_{m-b} = 83.706\,\text{pF/cm}$, and $C_{load} = 10\,\text{fF}$.

frequency is not above several tens of gigahertz [28]. Otherwise, it should be treated appropriately in the prediction of signal transmission characteristics.

5. CONCLUSION

According to different orders of approximation of the derived transfer function and the equivalent circuit model of SWCNT bundle interconnect, their stability as well as signal transmission characteristics is studied in this paper. It is indicated that the stability of a driven SWCNT bundle interconnect can be determined by, as we know, its extracted pole distribution diagram. Using the fourth-order approximation of the transfer function, the transmitted signal waveform in the SWCNT bundle interconnect can be captured accurately, in particular the signal overshoot and time delay. Also, compact expressions that describe the transient response of single and two coupled carbon nanotube bundle interconnects are presented to enable physical insight and accurate estimations of the time delay and crosstalk for carbon nanotube bundle interconnects.

ACKNOWLEDGMENT

The authors acknowledge the financial supports by the National Natural Science Fund under Grant 60801006 via Zhejiang University

of China. In particular, the authors sincerely appreciate Professor Venkatesan, Georgia Institute of Technology of USA, for providing part of C++ program used for our simulation.

REFERENCES

1. Li, H., C. Xu, N. Srivastava, and K. Banerjee, "Carbon nanomaterials for next-generation interconnects and passives: Physics, status, and prospects," *IEEE Trans. Electron. Device,* Vol. 56, No. 9, 1799–1821, Sep. 2009.
2. Burke, P. J., "An RF circuit model for carbon nanotubes," *IEEE Trans. Nanotech.*, 55–58, Mar. 2003.
3. Naeemi, A. and J. D. Meindl, "Compact physical model for multiwall carbon nanotube interconnect," *IEEE Trans. Electron. Device Lett.*, Vol. 27, No. 5, 338–340, May 2006.
4. Li, H., W. Y. Yin, K. Banerjee, and J. F. Mao, "Circuit modeling and performance analysis of multi-walled carbon nanotube interconnects," *IEEE Trans. Electron. Device,* Vol. 55, No. 6, 1328–1337, Jun. 2008.
5. Maffucci, A., G. Miano, and F. Villone, "A new circuit model for carbon nanotube interconnects with diameter-dependent parameters," *IEEE Trans. Nanotech.*, Vol. 8, No. 3, 345–354, May 2009.
6. Nieuwoudt, A. and Y. Massoud, "Understanding the impact of inductance in carbon nanotube bundles for VLSI interconnect using scalable modeling techniques," *IEEE Trans. Nanotech.*, Vol. 5, No. 6, 758–765, Nov. 2006.
7. Haruehanroengra, S. and W. Wang, "Analyzing conductance of mixed carbon-nanotube bundles for interconnect applications," *IEEE Electron. Device Lett.,* Vol. 28, No. 8, 756–759, Aug. 2007.
8. Wang, W., S. Haruehantoengra, L. Shang, and M. Liu, "Inductance of mixed carbon nanotube bundles," *Micro. & Nano. Lett.*, Vol. 2, No. 2, 35–39, Jun. 2007.
9. Rossi, D., J. M. Cazeaux, C. Metra, and F. Lombardi, "Modeling crosstalk effects in CNT bus architectures," *IEEE Trans. Nanotech.*, Vol. 6, No. 2, 133–145, Mar. 2007.
10. Pu, S. N., W. Y. Yin, J. F. Mao, and Q. H. Liu, "Crosstalk prediction of single- and double-walled carbon-nanotube (SWCNT/DWCNT) bundle interconnects," *IEEE Trans. Electron. Devices,* Vol. 55, No. 4, 560–568, Apr. 2009.
11. Naeemi, A., R. Sarvari, and J. D. Meindl, "Performance

comparison between carbon nanotube and copper interconnects for gigascale integration (GSI)," *IEEE Electron. Device Lett.*, Vol. 26, No. 2, 84–86, Feb. 2005.

12. Naeemi, A. and J. D. Meindl, "Design and performance modeling for single-walled carbon nanotubes as local, semi-global, and global interconnects in gigascale integrated systems," *IEEE Trans. Electron. Devices*, Vol. 54, No. 1, 26–37, 2007.
13. Srivastava, N., H. Li, F. Kreupl, and K. Banerjee, "On the applicability of single-walled carbon nanotubes as VLSI interconnects," *IEEE Trans. Nanotech.*, Vol. 8, No. 4, 542–559, Jul. 2009.
14. Fathi, D. and B. Forouzandeh, "A novel approach for stability analysis in carbon nanotube interconnects," *IEEE Electron. Device Lett.,* Vol. 30, No. 5, 475–477, May 2009.
15. Chen, W. C., W. Y. Yin, J. Lei, and Q. H. Liu, "Electrothermal characterization of single-walled carbon nanotube (SWCNT) interconnect arrays," *IEEE Trans. Nanotech.*, Vol. 8, No. 6, 718–728, 2009.
16. Patil, N., J. Deng, A. Lin, H. S. P. Wong, and S. Mitra, "Design methods for misaligned and mispositioned carbon-nanotube immune circuits," *IEEE Trans. Computer-aided Design of Integrated Circuits and Systems*, Vol. 27, No. 10, 1725–1746, Oct. 2008.
17. Close, G. F. and H. S. P. Wong, "Assembly and electrical characterization of multiwall carbon nanotube interconnects," *IEEE Trans. Nanotech.*, Vol. 7, No. 5, 596–600, Sep. 2008.
18. Patil, N., A. Lin, E. R. Myers, K. Ryu, A. Badmaev, C. W. Zhou, and H. S. P. Wong, "Wafer-scale growth and transfer of aligned single-walled carbon nanotubes," *IEEE Trans. Nanotech.*, Vol. 8, No. 4, 498–504, Jul. 2009.
19. Lin, A., N. Patil, H. Wei, S. Mitra, and H. S. P. Wong, "ACCNT-a metallic-CNT-tolerant design methodology for carbon-nanotube VLSI: concepts and experimental demonstration," *IEEE Trans. Electron. Device,* Vol. 56, No. 12, 2969–2978, Dec. 2009.
20. Banerjee, K. and A. Mehrotra, "Analysis of on-chip inductance effects for distributed RLC interconnects," *IEEE Trans. Computer-aided Designs of Integrated Circuits and Systems*, Vol. 21, No. 5, 904–915, Aug. 2002.
21. Davis, J. A. and J. D. Meindl, "Compact distributed RLC interconnect models — Part I: Single line transient, time delay, and overshoot expressions," *IEEE Trans. Electron. Device,* Vol. 47, No. 11, 2068–2077, Nov. 2000.

22. Davis, J. A. and J. D. Meindl, "Compact distributed RLC interconnect models — Part II: Coupled line transient expressions and peak crosstalk in multilevel networks," *IEEE Trans. Electron. Device*, Vol. 47, No. 11, 2078–2087, Nov. 2000.
23. Venkatesan, R., J. A. Davis, and J. D. Meindl, "Compact distributed RLC interconnect models — Part III: Transients in single and coupled lines with capacitive load termination," *IEEE Trans. Electron. Device,* Vol. 50, No. 4, 1081–1093, Apr. 2003.
24. Venkatesan, R., J. A. Davis, and J. D. Meindl, "Compact distributed RLC interconnect models — Part IV: Unified models for time delay, crosstalk, and repeater insertion," *IEEE Trans. Electron. Device,* Vol. 50, No. 4, 1094–1102, Apr. 2003.
25. Fathi, D. and B. Forouzandeh, "Time domain analysis of carbon nanotube interconnects based on distributed RLC model," *Nano.*, Vol. 4, No. 1, 13–21, 2009.
26. Fathi, D., B. Forouzandeh, S. Mohajerzadeh, and R. Sarvari, "Accurate analysis of carbon nanotube interconnects using transmission line model," *Micro & Nano Lett.*, Vol. 4, No. 2, 116–121, 2009.
27. Davis, J. A., "A hierarchy of interconnect limits and opportunities for gigascale integration (GSI)," Ph.D. dissertation, Univ. Georgia Institute of Technology, Mar. 1999.
28. Sarto, M. S., A. Tamburrano, and M. D'Amore, "New electron-waveguide-based modeling for carbon nanotube interconnects," *IEEE Trans. Nanotechnology*, Vol. 8, No. 2, 214–225, 2008.
29. Raguraman, V., "Multilevel interconnect architectures for gigascale integration (GSI)," Ph.D. dissertation, Georgia Institute of Technology, Feb. 2003.
30. Khalaj-Amirhosseini, M., "Closed form solutions for nonuniform transmission lines," *Progress In Electromagnetics Research B*, Vol. 2, 243–258, 2008.
31. Chiu, C.-N. and I.-T. Chiang, "A fast approach for simulating long-time response of high-speed dispersive and lossy interconnects terminated with nonlinear loads," *Progress In Electromagnetics Research*, PIER 91, 153–171, 2009.
32. Wang, Y. J., W. J. Koh, C. K. Lee, and K. Y. See, "Electromagnetic coupling analysis of transient signal through slots or apertures perforated in a shielding metallic enclosure using FDTD methodology," *Progress In Electromagnetics Research*, PIER 36, 247–264, 2002.